

Measurement of Nanoparticle Concentration Using Quartz Crystal Microgravimetry[†]

Vytas Reipa,^{*,‡} Geoffrey Purdum,[§] and Jonghoon Choi^{||}

Biochemical Science Division, National Institute of Standards and Technology, Gaithersburg, Maryland 20899, Department of Chemical Engineering, University of Massachusetts, Amherst, Massachusetts 01003, and Department of Chemical Engineering, Massachusetts Institute of Technology, Cambridge, Massachusetts 02139

Received: April 28, 2010; Revised Manuscript Received: August 31, 2010

Various nanoscale items (e.g., nanoparticles and nanotubes) have been actively investigated due to their unique physicochemical properties. A common issue encountered in such studies is accurate expression of nanoparticle concentration. Given the critical importance of the dose–response relationship, we present the use of quartz crystal microgravimetry (QCM) to accurately measure nanoparticle concentration in a colloidal suspension. Application of a small drop of the nanoparticle suspension in a volatile solvent to the crystal surface leaves a dry nanoparticle residue after solvent evaporation after which the shift in the crystal resonant frequency is recorded. The instrument was calibrated using a set of serial dilutions of Si and Ag nanopowder in methanol, rhodamine B in methanol, and ferrocene in cyclohexane. Using QCM, a linear response for nanoparticle concentrations up to 1300 $\mu\text{g/mL}$ was determined. The developed method was used to determine the concentrations of size-selected, octyl-terminated Si nanocrystal samples with median diameters in the range 1.1–14.8 nm and also to calculate size-dependent nanocrystal extinction coefficients.

Introduction

Some of the most dynamic areas of study for nanoparticles are motivated by the incredible potential applications of these materials as drug delivery agents,^{1,2} biological labels and contrast agents,^{3,4} UV protection screens,⁵ solid state lighting, and energy sources.^{6,7} Recently, concerns with nanomaterial toxicity have stimulated numerous investigations into the interactions of nanoparticles with biological systems.^{8,9} A common issue encountered in such studies is accurate nanoparticle concentration expression,¹⁰ given the critical importance of the dose–response relationship. Furthermore, particle concentration can be alternatively expressed as mass, number of particles (molar), or surface area units, often complicating interstudy comparisons.

Accurate gravimetric measurement using analytical balances may not be practical in the submicrogram range, as this is approaching the sensitivity limit for most instruments. Therefore, indirect methods, such as TEM image analysis,¹¹ often provide approximate concentration assessments, but these methods are rather labor intensive and may require expensive instrumentation. To obtain a TEM image, a fixed volume of a particle colloid sample is deposited on a TEM grid and the particles are counted per unit of the grid area after drying. In this way, a typical TEM image, containing up to several thousand particles, should accurately represent the full sample batch, a task not easily achievable in heterogeneous particle mixtures possessing considerable variation in size, shape, and aggregation. Particle losses during drying and grid transfer to the vacuum chamber, however, are typically not accounted for in this method.

Most applications require knowledge of the nanoparticle concentration in solution or a given medium. Optical absorbance is a relatively simple nanoparticle concentration measurement, provided

particle molar extinction coefficients are available.¹² Application of Beer's law, however, is not always possible for semiconducting quantum dots due to bandgap variation of the particle size in the quantum confinement size range and resulting uncertainties in the absorption cross section.^{13,14} Additionally, sensitivity of optical properties to the particle chemical environment and light scattering¹⁵ may further complicate numerical nanoparticle concentration assessments using solution absorbance measurements. Nevertheless, CdTe, CdSe, and CdS extinction coefficients have been recently determined^{12,16,17} for various particle sizes and absorbance measurements can therefore be employed in these quantum dot concentration measurements.

Silicon nanocrystals display intense photoluminescence spanning from the UV to the near IR in the quantum confinement range (at $d < 5$ nm) and have generated considerable interest for biological applications.^{8,18,19} In particular, the nontoxic nature of the material may significantly expand their application compared to type III–V and II–VI semiconductor quantum dots that typically require a robust protective shell to prevent the leaching of toxic core materials.²⁰ Assessing Si nanocrystal concentration from colloidal suspension absorbance is hampered by the lack of reliable extinction coefficient values due to the variation in particle size.¹⁴ Therefore, measurement of the nanocrystal size distribution is essential in relating absorbance to nanoparticle concentration. Moreover, nanoparticle optical properties are significantly affected by the extent of surface atom passivation.^{18,21} These characteristics complicate the measurement of silicon nanoparticle concentration using simple colloid absorptivity.

The quartz crystal microbalance (QCM) is a nanogram resolution mass sensing technique based on the piezoelectric effect.^{22,23} The technique is quite versatile, as it possesses a wide detection range and can be applied to deposit mass measurements in the gas or liquid phase. Deposition of a liquid drop on one of the faces of an oscillating crystal causes a shift in its resonant frequency, enabling accurate residue film mass measurements following solvent evaporation.²⁴ We explore here the

[†] Part of the "Robert A. Albery Festschrift".

* Corresponding author.

[‡] National Institute of Standards and Technology.

[§] University of Massachusetts.

^{||} Massachusetts Institute of Technology.

application of quartz crystal microgravimetry to accurately quantify nanoparticle concentrations in size-selected colloidal suspensions in a low boiling point solvent. By depositing a fixed volume of the nanoparticle colloidal solution and determining the dry residue mass after solvent evaporation, we measured the nanoparticle concentration and expressed it in mass per unit volume. Concentration data on size-selected Si nanocrystal batches enabled the calculation of the Si nanocrystal extinction coefficient and may help in practical applications of absorption-based nanoparticle concentration determination when accurate quantitation of a small nanocrystal sample is required.

Experimental Section

Preparation of Si Nanoparticles. Silicon wafers were electrochemically etched in a HF:H₂O:ethanol (1:1:2, volume ratio) mixture by following the lateral etching procedure.²⁵ Polished wafers (<111> oriented, 0.001–0.01 ohm-cm, As-doped) were purchased from Virginia Semiconductor, Inc., Fredericksburg, VA. (Certain commercial equipment, instruments, materials, or companies are identified in this paper to specify adequately the experimental procedure. In no case such identification does imply recommendation or endorsement by the National Institute of Standards and Technology, nor does it imply that the materials or equipment are necessarily the best available for the purpose.) Anodic etching was performed in a Teflon cell that accommodates a 100 mm diameter Si wafer placed between two Si cathodes. Electric contact was provided to the top edge of the vertically mounted wafer and electrolyte was slowly pumped into the cell, hence providing a moving electrolyte boundary. The total etch time typically was about 4 h per 100 mm diameter wafer at 120 mA constant current, supplied by a galvanostat (Model 363, EG&G Inc., Princeton, NJ). After anodic etching, the wafer was washed several times in deionized water and then methanol (HPLC grade, Mallinckrodt Chemicals, Phillipsburg, NJ) and blow-dried with nitrogen gas. Dry wafers displayed an intense orange-red luminescence under 365 nm UV lamp excitation. Next, Si wafers were subjected to 30 min of sonication in deaerated pure toluene (Sigma Inc.) under vigorous N₂ purging. The resulting suspension displayed broadband photoluminescence (PL) in the orange/red spectral range under UV (365 nm) excitation. Surface atom hydrogen termination of silicon nanoparticles in toluene solvent was replaced by octyl through a photocatalyzed hydrosilylation reaction. A typical procedure includes mixing the silicon nanoparticle toluene dispersion with 1-octene at 10:1 volume ratio, placing it in a UV reactor (model RMR-600, Rayonet, Branford, CT), and exposing it to 254 nm light for periods from 30 min to 12 h under vigorous N₂ purging. Octyl-passivated Si nanoparticle solution was completely dried in a N₂ stream and redispersed in toluene. The resulting nanoparticle surface termination was verified using FTIR spectroscopy. All colloidal solutions were sequentially filtered several times through 100 and 20 nm syringe filters (Anotop, Whatman) prior to measurements.

Quartz Crystal Microbalance Measurements. Chromium/gold electrode quartz crystal (polished, 1 in. diameter, dry frequency of 5 MHz, AT-cut) was used as a sensor crystal. The microbalance (Model QCM200, Stanford Research Systems Inc., Sunnyvale, CA) was enclosed in a metal box to minimize interferences from ambient air movement. Typically, 20 μ L drops of the nanoparticle suspension were deposited on the sensor crystal using a gas-tight microsyringe (Hamilton Co., Reno, NV) and then solvent was allowed to evaporate while the QCM resonant frequency and oscillation resistance variation

were continuously recorded. Following the complete solvent evaporation, a stabilized resonance frequency was recorded. The dilution series of commercial Si and Ag nanopowders (Sigma Aldrich Inc., St. Louis, MO, cat.# 633097) with particle concentrations from 0.1 to 6000 μ g/mL were prepared in methanol using a calibrated analytical balance (Ohaus Inc., Pine Brook, NJ) and ultrasonic agitation. A plot of the resonance frequency vs gravimetrically determined Si nanoparticle concentration in methanol suspension was used to make a standard curve by fitting to a linear function. Additional calibration was provided using solutions of rhodamine B in methanol and ferrocene in cyclohexane (Sigma Aldrich, St. Louis, MO). Dye concentrations in solution were determined from the absorbance measurements in a 1 cm quartz cell. The quartz crystal was replaced after each measurement, sonicated in neat toluene for 30 min, and dried in a gentle N₂ stream. All experiments were performed at room temperature and atmospheric pressure.

Absorbance Measurements. The nanoparticle and organic dye solutions were contained in 10 mm optical path length quartz cells (NSG, Inc.) for UV–vis absorbance measurements. Spectra were recorded in the range 200–800 nm at room temperature using a two-channel spectrophotometer (Perkin-Elmer, Lambda 850) with pure solvent as a reference. Samples were diluted with pure solvents so the maximum absorbance did not exceed 2 absorbance units.

Particle Size Measurement. Si nanocrystal colloidal samples were size-selected by varying the exposure to UV light during the hydrosilylation reaction, and particle size was determined using photon correlation spectroscopy (model 90 Plus, Brookhaven Instruments Co., Holtsville, NY) with the detector at 90° and at room temperature. Size distribution was fit to the log-normal function by multimodal size distribution analysis software. Nanoparticle colloidal solutions for these measurements were concentrated up to about 0.5 mg/mL to optimize the detector photon counting rate.

HRTEM images were obtained by depositing a small drop of Si nanoparticle colloidal solution in toluene on a carbon grid, using a JEOL JEM-2010 instrument (JEOL Ltd., Tokyo, Japan) operated at $U = 200$ kV.

Results and Discussion

QCM Calibration. The goal of this study was to measure the mass and molar concentrations of nanoparticles in a colloidal solution. Quartz crystal microgravimetry of the dry nanoparticle powder following total solvent evaporation was investigated and compared to concentration estimates from conventional gravimetry and UV–vis absorbance measurements. A 20 μ L drop of the volatile solvent based nanocolloid was applied to the center of the horizontally positioned quartz crystal (area, $A = 4.9$ cm², Figure 1). The drop spread across the entire crystal surface to leave a dry residue after complete solvent evaporation. Typical frequency–time dependence plots, recorded following pure methanol application, are shown in Figure 2. When the liquid drop was deposited with a syringe (indicated by vertical arrows on Figure 2), the frequency rapidly dropped approximately 800 Hz, followed by oscillation during solvent evaporation (Figure 2). The crystal frequency then recovered to the predeposition value in 3–5 min, demonstrating the absence of any residual film on the crystal surface. We have tested several low boiling point solvents compatible with QCM housing materials (methanol, ethanol, toluene, hexane, and cyclohexane) and observed crystal resonance frequency recovery to within 3 Hz of the predeposition value following complete solvent evaporation. The frequency–time profiles and drying rates were found to vary

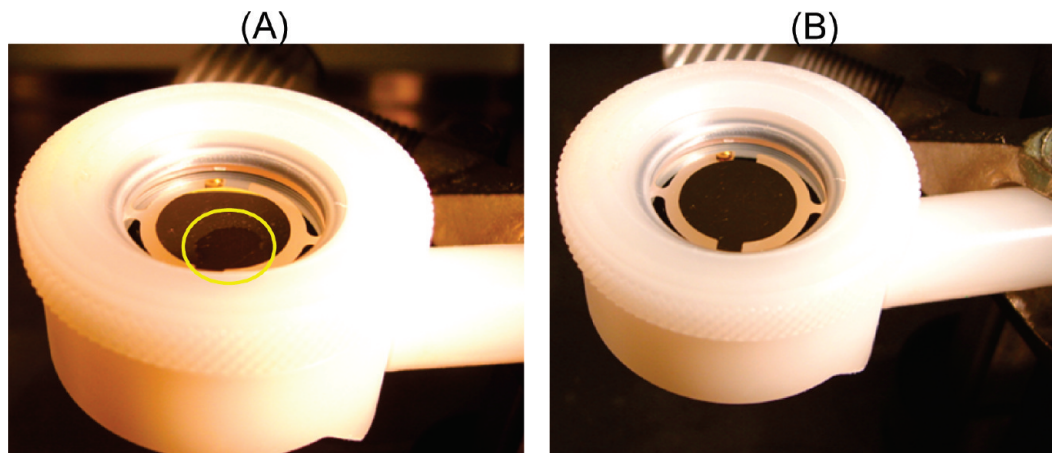


Figure 1. Quartz crystal images: (A) following the application of a nanocrystal colloidal suspension, circle indicates residual solvent; (B) following complete solvent evaporation.

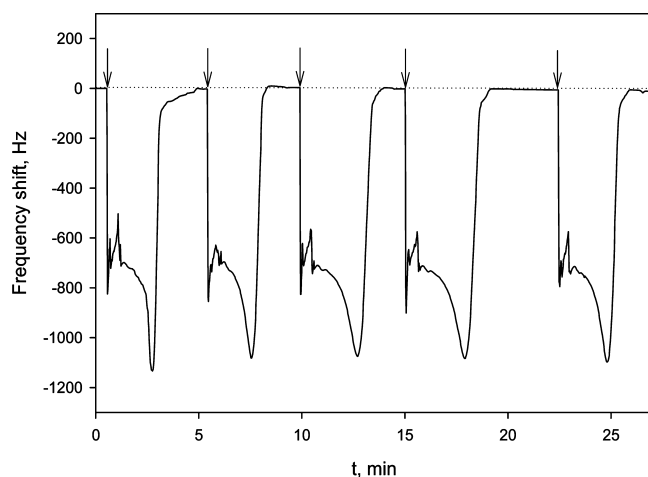


Figure 2. Series of quartz crystal resonance frequency traces during the application of pure methanol and drying. 20 μL methanol drops were deposited on the crystal surface using a gas-tight syringe at the times indicated by arrows.

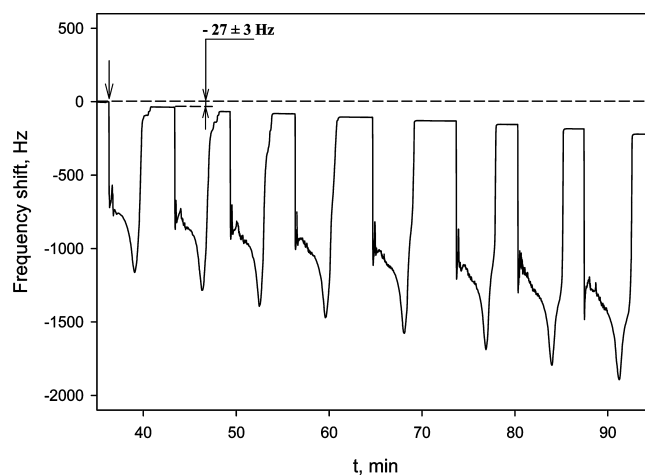


Figure 3. QCM frequency trace recorded during the sequential injection of 20 μL drops of methanol containing 120 $\mu\text{g}/\text{mL}$ silicon nanoparticles. The presence of dry nanoparticle residue after methanol evaporation decreases the crystal resonance frequency by 27 Hz.

for the different solvents and application volumes. Deionized water was also tested as a solvent, but the complete evaporation of the drop under our conditions ($t = 20\text{ }^\circ\text{C}$ and atmospheric pressure) took up to 40 min. The deposited solvent volume in these experiments was limited to 20 μL by our crystal surface area ($S = 4.91\text{ cm}^2$), as the entire applied liquid mass had to be contained on the crystal surface during evaporation to avoid particulate loss on the crystal holder wall surface (Figure 1).

For QCM calibration with commercial nanoparticles, we chose methanol, as it offered a uniform liquid film throughout the entire crystal face, rapidly evaporated, and had the adequate solubility of the nanoparticles. Figure 3 shows the microbalance response to 120 $\mu\text{g}/\text{mL}$ Si nanoparticles in methanol under identical deposition conditions as those used for the data in Figure 2. Multiple colloidal solution applications showed that the lower resonance frequency plateau after each deposition was due to the residual mass of the dry Si nanoparticle film. The steps are $27 \pm 3\text{ Hz}$ and correspond to 11.3 Hz/ μg of the nanoparticle mass in suspension.

The microbalance was calibrated to determine the Sauerbrey equation applicability range. First, a stock solution was prepared from a dry powder weighed on an analytical balance and dispersed in methanol using mild sonication. Next, a series of 20 μL pure methanol drops were deposited and evaporated to determine instrument noise level and reproducibility. Finally, a

series of 20 μL Si and Ag nanoparticle suspension drops (particle concentration ranged from 5 to 6000 $\mu\text{g}/\text{mL}$) in methanol were deposited and plateau frequencies were recorded (Figure 3). A standard curve (Figure 4) indicated that the QCM frequency responded linearly to dry nanoparticle loading up to $c = 1300\text{ }\mu\text{g}/\text{mL}$.

Deviations from Sauerbrey's relation (shown as a solid line in Figure 4) at the nanoparticle loading above 1300 $\mu\text{g}/\text{mL}$ were likely due to the decoupling of the thick nanopowder film from the shear vibrational modes of the AT-cut crystal.²² Measurements at concentrations less than 5 $\mu\text{g}/\text{mL}$ were irreproducible with 1 s crystal frequency integration time and indicated the practical lower limit of the QCM gravimetry under these experimental conditions. However, at least one order of magnitude lower nanoparticle concentration could be measured reliably with the increase of the QCM frequency integration time or multiple sample applications as frequency shifts were additive up to the upper crystal mass loading of about 270 $\mu\text{g}/\text{cm}^2$.

Octyl-Passivated Si Nanocrystal Concentration Measurement. A sample of typical QCM frequency–time traces, following the application of 20 μL of octyl-passivated size-selected Si nanocrystals in toluene is shown in Figure 5. The crystal series resonance resistance R that provides information on the viscoelastic properties of bound mass was monitored

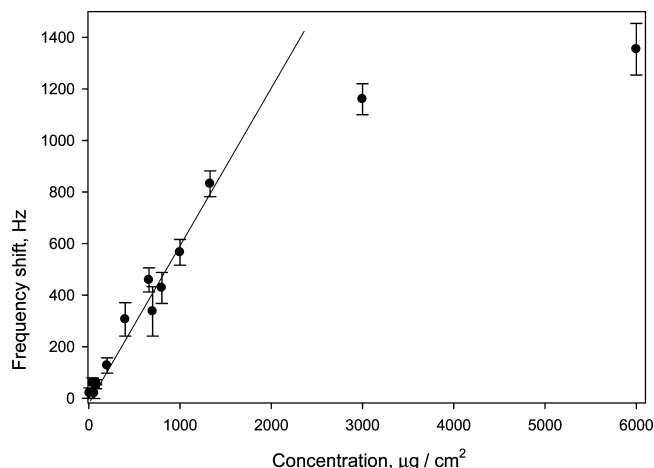


Figure 4. QCM calibration obtained from dilution series of Si and Ag nanoparticles in methanol (full dots). The solid line represents the frequency shift estimate from Sauerbrey's relation. Error bars correspond to one standard deviation from at least 20 measurements.

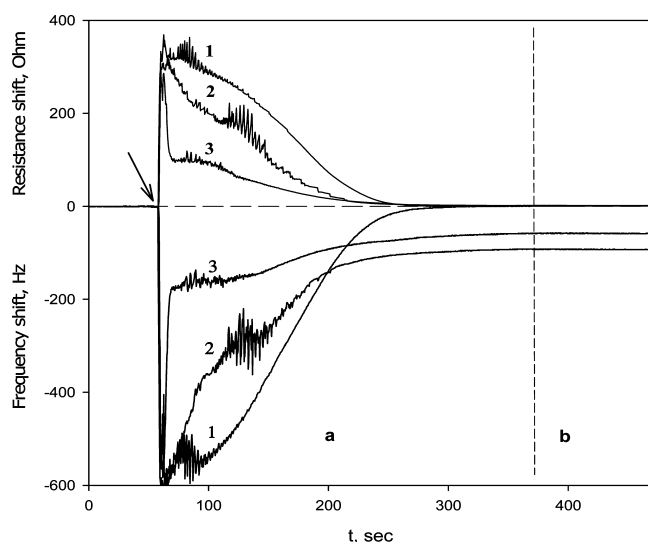


Figure 5. Series of quartz microbalance frequency-time and series resonance resistance-time traces, recorded following the application (as indicated by an arrow) of 20 μL of octyl-passivated Si nanocrystal colloidal suspension in toluene. Suspension particle concentration ($\mu\text{g}/\text{mL}$): (1) 0, (2) 194, (3) 148.

together with the resonance frequency. In our experiments, it presents a convenient indicator of the solvent evaporation stage (shown in the upper panel of Figure 5), since dry nanoparticle film typically represents the elastic mass bound tightly to the QCM surface, as demonstrated by negligible ΔR residual values.

Following the solvent drop application a gradual frequency (f) and series resonance resistance (R) recovery indicates solvent evaporation, which continues for about 5 min (interval a in Figure 5). A serial resistance drop to the predeposition value

follows the loss of the liquid film, and the frequency plateau reveals the presence of the dry nanoparticle powder mass loading (interval b) that is used to calculate nanoparticle concentration in the suspension. On the basis of instrument calibration with commercial Si and Ag nanopowders dispersed in methanol (Figure 4), the total dry nanoparticle mass can be estimated and the solution concentration calculated from Sauerbrey's equation for suspensions up to 1300 $\mu\text{g}/\text{mL}$

$$\Delta f = -C_f \Delta m \quad (1)$$

where Δf is the observed residual frequency change (Hz), Δm is the change in mass per unit area ($\mu\text{g}/\text{cm}^2$), and C_f is the crystal sensitivity factor ($56.6 \text{ Hz } \mu\text{g}^{-1} \text{ cm}^2$). The nanoparticle concentration c_m in the suspension drop of volume v then is calculated from

$$c_m = \frac{\Delta m S}{v} \quad (2)$$

where $S = 4.91 \text{ cm}^2$ is the quartz crystal surface area.

Molar Concentration and Si Nanocrystal Extinction Coefficient. Knowledge of the Si nanocrystal extinction coefficient is necessary in particle molar concentration measurement using the colloidal solution absorbance reading. However, the direct measurement of the extinction coefficient using Beer's law is complicated by its variation with nanoparticle size and unknown number of absorbing nanocrystals (molar concentration). We prepared five size-selected samples of the octyl-terminated Si nanocolloid in toluene by varying the UV treatment conditions in the hydrosilylation solutions, measured particle mass concentrations using the above QCM procedure, and determined particle size distribution profiles by means of dynamic light scattering (DLS). Next, using the approach described in ref 17, we calculated molar particle concentrations and estimated the extinction coefficients at 300 and 340 nm (Table 1). Briefly, the particle number in the volume unit was calculated from the particle size and mass concentration data. The overall silicon mass of the sample was obtained by subtracting the octyl monolayer weight from the total measured nanocrystal mass QCM reading. Octyl monolayer mass was determined using thermogravimetry under a nitrogen atmosphere. A typical mass vs temperature curve, recorded during temperature ramp up to 600 $^\circ\text{C}$ is shown in Figure 6. Particle weight loss due to burnout of the organic shell indicated that the octyl monolayer coverage varied from 76% (at $d = 1.1 \text{ nm}$) to 58% (at $d = 14.8 \text{ nm}$) when estimated from

$$\theta = \frac{3}{4\pi[(r+d)^3 - r^3]\rho_{\text{shell}}} m \quad (3)$$

TABLE 1: Size-Selected Si Nanocrystal Molar (ϵ) and Mass Based (μ) Extinction Coefficients and Absorption Cross Section (σ) at 300 and 340 nm

| sample ID | diameter (nm) | $\lambda = 300 \text{ nm}$ | | | $\lambda = 340 \text{ nm}$ | | |
|-----------|---------------|--|--|----------------------------|--|--|----------------------------|
| | | ϵ ($\text{M}^{-1} \text{ cm}^{-1}$) | μ ($\text{g}^{-1} \text{ cm}^2$) | σ (cm^2) | ϵ ($\text{M}^{-1} \text{ cm}^{-1}$) | μ ($\text{g}^{-1} \text{ cm}^2$) | σ (cm^2) |
| 1 | 14.8 | 8.36×10^6 | 3.5 | 3.20×10^{-14} | 1.38×10^6 | 0.58 | 5.27×10^{-15} |
| 2 | 7.1 | 8.46×10^5 | 3.2 | 3.24×10^{-15} | 1.91×10^5 | 0.73 | 7.31×10^{-16} |
| 3 | 5.2 | 4.51×10^5 | 4.4 | 1.73×10^{-15} | 1.28×10^5 | 1.25 | 4.92×10^{-16} |
| 4 | 1.4 | 1.48×10^5 | 73.1 | 5.66×10^{-16} | 2.80×10^4 | 13.8 | 1.07×10^{-16} |
| 5 | 1.1 | 1.23×10^5 | 125.1 | 4.7×10^{-16} | 2.38×10^4 | 24.2 | 9.09×10^{-17} |

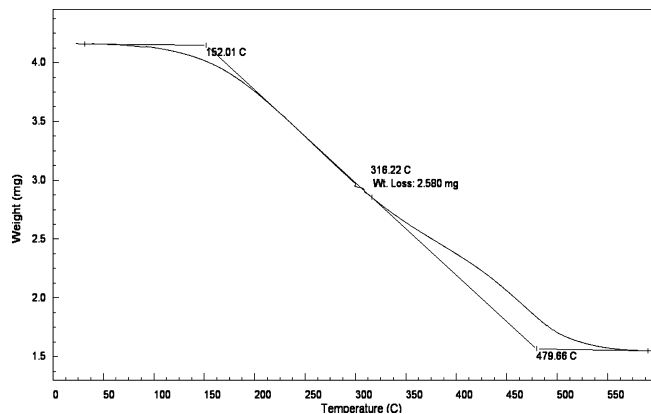


Figure 6. Thermogravimetric analysis curve of octyl-passivated Si NP sample under N_2 atmosphere. Initial sample mass $m = 4.1721$ mg, median particle diameter $d = 1.4$ nm.

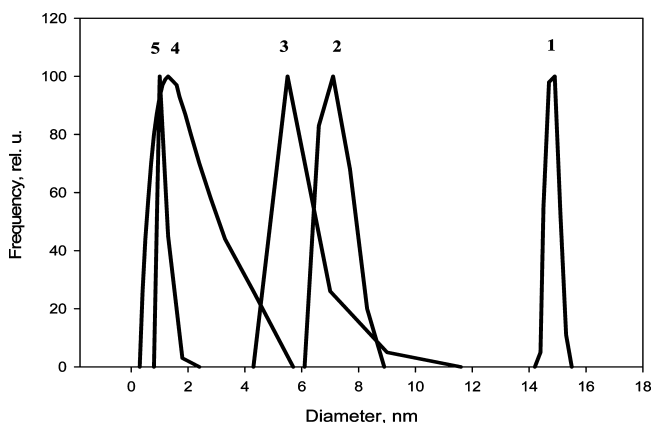


Figure 7. Size distribution of the five size-selected Si nanocrystal samples obtained from the DLS.

Here, r is the median particle core radius, $d = 1.2$ nm is the octyl shell thickness, θ is the octyl surface coverage, m is the relative mass loss from the thermogravimetry experiment, and ρ_{shell} is the density of the octyl coating, assumed to be close to that of polystyrene, 1.12 g/cm^3 .²⁶

The number concentration of particles is equal to the content of total Si divided by the number of Si atoms per particle (N_{Si})

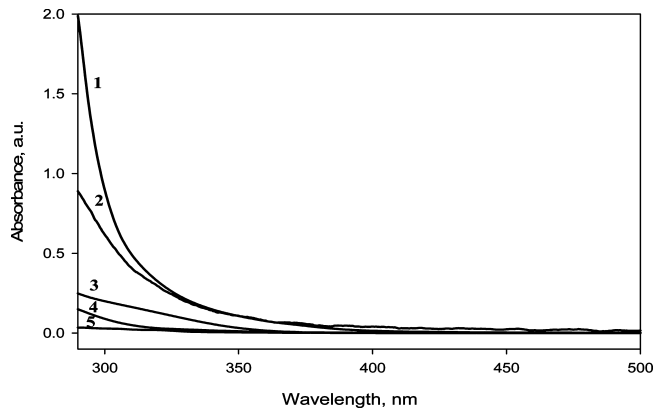
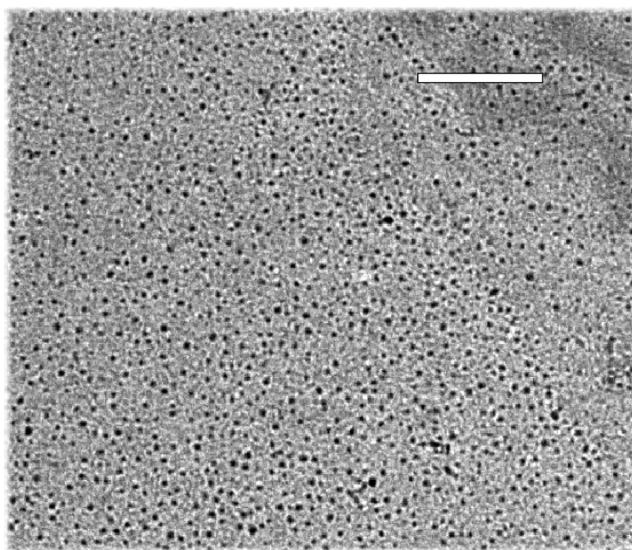


Figure 9. Absorbance of the size-selected octyl-passivated Si nanocrystal samples.

that can be obtained from the median particle core radius r and the volume of the bulk silicon unit cell $V_{\text{unit}} = 160 \text{ \AA}^3$ containing 8 Si atoms

$$N_{\text{Si}} = \frac{4}{3}\pi r^3 \frac{8}{V_{\text{unit}}} \quad (4)$$

Our five Si nanocrystal samples had log-normal size distributions (DLS data) with median core diameters of 1.1, 1.4, 5.2, 7.1, and 14.8 nm (Figure 7) at mass concentrations of 59, 503, 430, 408, and 298 $\mu\text{g/mL}$, respectively. Silicon core diameters were obtained by subtracting the fully extended octyl shell thickness ($d = 1.2$ nm) from the measured hydrodynamic particle radius. Given the sensitivity of particle molar concentration estimates on the particle core diameter measurement (eq 4), we have validated the DLS result using the HRTEM images of selected colloidal samples (Figure 8). Median particle diameters obtained from both methods are rather close (compare sample #4 in Figure 7 and the right panel of Figure 8); however, size distribution profiles differed in shape, since TEM image analysis discounted particles with diameters less than 1 nm.

Absorbance measurements of 10 times diluted samples (Figure 9) were used to estimate the molar based extinction coefficient for Si nanoparticles at 300 and 340 nm according to

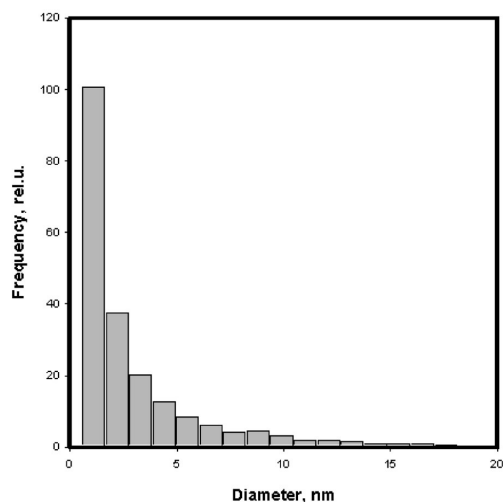


Figure 8. HRTEM image of the octyl-passivated Si nanoparticle sample #4 (left panel). The size bar corresponds to 50 nm. Particle size distribution histogram of the 1350 particles obtained using the image analysis (right panel).

Beer's law, $\epsilon_\lambda = A_\lambda/cl$, where c is the particle molar concentration and l is the path length in cm. Mass based extinction coefficient values μ_λ were also included in Table 1, as they are less reliant on accurate size distribution measurement.

When the particle diameter (d) is much smaller than the wavelength of light in a selected medium (expressed as λ/n_1 , where λ is the vacuum wavelength and $n_1 = 1.58$ is the index of refraction of toluene²⁷), the scattering can be neglected and the extinction coefficient (in $M^{-1} \text{ cm}^{-1}$) is converted to a per particle absorption cross section,¹⁷ expressed in cm^2

$$\sigma_\lambda = \frac{2303\epsilon_\lambda}{N_A} \quad (5)$$

where N_A is Avogadro's number.

The extinction coefficient values in Table 1 increase with the Si nanocrystal size, as has been reported for binary semiconductor quantum dots.^{12,17} Table 1 contains ϵ_λ and μ_λ values for 300 and 340 nm, as toluene absorbance interferes with Si nanoparticle absorbance measurement below 290 nm. For practical concentration measurements using Beer's law in small Si nanoparticle ($d < 5$ nm) colloidal solutions, ϵ_{300} would be more appropriate than ϵ_{340} with the absorbance edge blue shift due to quantum confinement²⁸ and resulting negligible absorbance of smaller particles at 340 nm (Figure 9). The absorbance cross section σ_λ reflects the strength of the given optical transition, and our values are comparable to data for Si nanocrystals obtained by Kovalev et al. from photoluminescence Auger saturation experiments,¹⁴ chemically synthesized alkylated Si nanocrystals,²⁹ and estimates using the formalism suggested in ref 17 for CdSe.

The experimental errors of our nanoparticle concentration measurements primarily originate from the colloid pipeting errors (estimated not to exceed 5%) and particle size distribution measurement. Molar nanoparticle concentration estimates are distinctively sensitive to the measured size as particle mass scales as a cube of diameter. As both DLS and TEM have a lower sensitivity limit around 1 nm, uncertainties in molar concentration are higher for particles in this size range (samples #4 and #5 in Table 1). Therefore, for polydisperse nanoparticle sample concentration measurements from absorbance spectra, a mass based extinction coefficient (μ) would be preferable. As particle absorption cross section σ rises nonlinearly with the particle diameter (Table 1); even a small proportion of larger particles in polydisperse colloidal samples could markedly increase the measured σ values. Therefore, a standard deviation of $\pm 20\%$ is estimated for the values of ϵ , μ , and σ in Table 1.

In summary, we have demonstrated a practical way to measure nanoparticle concentration in a colloidal solution using quartz crystal microgravimetry. Application of a small drop of the nanoparticle colloid in a volatile organic solvent to the crystal surface leaves a dry nanoparticle film after solvent evaporation. Crystal resonant frequency shifts obeyed Sauerbrey's equation for the dry nanoparticle concentrations up to 1300 $\mu\text{g/mL}$, as

calibrated using a set of serial dilutions of Si and Ag nanopowders in methanol, rhodamine B in methanol, and ferrocene in cyclohexane. Utility of QCM microgravimetry was shown in determining the molar concentrations of five size-selected Si nanocrystal samples with median diameters of 1.1, 1.4, 5.2, 7.1, and 14.8 nm and calculating size-dependent nanocrystal extinction coefficients.

Acknowledgment. We thank Dr. Taeho Kim for his assistance with nanoparticle HRTEM imaging and Dr. Brian Lang for thermogravimetry measurements. This work was partially supported by the NIST standard reference data program.

References and Notes

- (1) Prestidge, C. A.; Barnes, T. J.; Lau, H.; Barnett, C.; Loni, A.; Canham, L. *Expert Opin. Drug Delivery* **2007**, *4*, 101.
- (2) Kneuer, C.; Sameti, M.; Bakowsky, U.; Schiestel, U.; Schirra, H.; Lehr, C. M. *Bioconjugate Chem.* **2000**, *11*, 926.
- (3) Smith, A. M.; Ruan, G.; Rhyner, M. N.; Nie, S. *Ann. Biomed. Eng.* **2006**, *34*, 3.
- (4) Bruchez, M.; Moronne, M.; Gin, P.; Weiss, S.; Alivisatos, P. A. *Science* **1998**, *281*, 2013.
- (5) Nohynek, G. J.; Lademann, J.; Ribaud, C.; Roberts, M. S. *Crit. Rev. Toxicol.* **2007**, *37*, 251.
- (6) Hanna, M. C.; Nozik, A. J. *J. Appl. Phys.* **2006**, *100*, 074510.
- (7) Stupca, M.; Alsalhi, M.; Al Saud, T.; Almuhan, A.; Nayfeh, M. H. *Appl. Phys. Lett.* **2007**, *91*, 063107.
- (8) O'Farrell, N.; Houlton, A.; Horrocks, R. B. *Int. J. Nanomed.* **2006**, *1*, 451.
- (9) Nel, A.; Xia, T.; Madler, L.; Li, N. *Science* **2006**, *311*, 622.
- (10) Buzea, C.; Pacheco, I. I.; Robbie, K. *Biointerphases* **2007**, *2*, MR17.
- (11) Pyrz, W. D.; Buttrey, D. J. *Langmuir* **2008**, *24*, 11350.
- (12) Yu, W. W.; Qu, L.; Guo, W.; Peng, X. *Chem. Mater.* **2003**, *14*, 2854.
- (13) Jacobsohn, M.; Banin, U. *J. Phys. Chem. B* **2000**, *104*, 1.
- (14) Kovalev, D.; Diener, J.; Heckler, H.; Polisski, G.; Kunzner, N.; Koch, F. *Phys. Rev. B* **2000**, *61*, 4485.
- (15) Eckhoff, D. A.; Sutin, J. D. B.; Clegg, R. M.; Gratton, E.; Rogozhina, E. V.; Braun, P. V. *J. Phys. Chem. B* **2005**, *109*, 19786.
- (16) Dai, Q.; Wang, Y.; Li, X.; Zhang, Y.; Pellegrino, D. J.; Zhao, M.; Zou, B.; Seo, J. T.; Wang, Y.; Yu, W. W. *ACS Nano* **2009**, *3*, 1518.
- (17) Leatherdale, C. A.; Woo, W.-K.; Mikulec, F. V.; Bawendi, M. G. *J. Phys. Chem. B* **2002**, *106*, 7619.
- (18) Choi, J.; Zhang, Q.; Reipa, V.; Wang, N. S.; Stratmeyer, M. E.; Hitchins, V. M.; Goering, P. L. *J. Appl. Toxicol.* **2009**, *29*, 52.
- (19) Erogbogbo, F.; Yong, K. T.; Roy, I.; Xu, G. X.; Prasad, P. N.; Swihart, M. T. *ACS Nano* **2008**, *2*, 873.
- (20) Derfus, A. M.; Chan, W. C. W.; Bhatia, S. N. *Nano Lett.* **2004**, *4*, 11.
- (21) Vasiliev, I.; Chelikovskiy, J. R.; Martin, R. M. *Phys. Rev. B* **2002**, *65*, 121302.
- (22) Guilbault, G. G.; Jordan, J. M. *Crit. Rev. Anal. Chem.* **1988**, *19*, 1.
- (23) Marx, K. A. *Biomacromolecules* **2003**, *5*, 1099.
- (24) Schulz, W. W.; King, W. H. *J. Chromatogr. Sci.* **1973**, *11*, 343.
- (25) Choi, J.; Wang, N. S.; Reipa, V. *Langmuir* **2007**, *23*, 3388.
- (26) *CRS Handbook of Chemistry and Physics*, 87th ed.; Lide, D., Ed.; CRC Press: Boca Raton, FL, 2006–2007.
- (27) Marsh, K. N., Ed. *Recommended Reference Materials for the realization of Physicochemical Properties*; Blackwell Scientific Publications: Oxford, U.K., 1987.
- (28) Meier, C.; Gondorf, A.; Lutjohann, S.; Lorke, A.; Wiggers, H. *J. Appl. Phys.* **2007**, *101*, 103112.
- (29) Rosso-Vasic, M.; Spruijt, E.; Van Lagen, B.; Cola, L. D.; Zuilhof, H. *Small* **2008**, *4*, 1835.